arXiv:1404.0415v2 [cond-mat.mes-hall] 1 Jul 2014

Calculations of magnetic states and minimum energy paths of transitions using a noncollinear extension of the Alexander-Anderson model and a magnetic force theorem

Pavel F. Bessarab[1,2], Valery M. Uzdin[2,3], and Hannes Jónsson[1,4]

[1]*Science Institute and Faculty of Physical Sciences, VR-III, University of Iceland, 107 Reykjavík, Iceland*

[2]*Department of Physics, St. Petersburg State University, St. Petersburg, 198504, Russia*

[3]*St.Petersburg National Research University of Information Technologies, Mechanics and Optics, St. Petersburg, 197101, Russia and*

[4]*Dept. of Applied Physics, Aalto University, Espoo, FI-00076, Finland*

(Dated: July 2, 2014)

Abstract

Calculations of stable and metastable magnetic states as well as minimum energy paths for transitions between states are carried out using a noncollinear extension of the multiple-impurity Alexander-Anderson model and a magnetic force theorem which is derived and used to evaluate the total energy gradient with respect to orientation of magnetic moments – an important tool for efficient navigation on the energy surface. By using this force theorem, the search for stable and metastable magnetic states as well as minimum energy paths revealing the mechanism and activation energy of transitions can be carried out efficiently. For Fe monolayer on W(110) surface, the model gives magnetic moment as well as exchange coupling between nearest and next-nearest neighbors that are in good agreement with previous density functional theory calculations. When applied to nanoscale Fe islands on this surface, the magnetic moment is predicted to be 10% larger for atoms at the island rim, explaining in part an experimentally observed trend in the energy barrier for magnetization reversal in small islands. Surprisingly, the magnetic moment of the atoms does not change much along the minimum energy path for the transitions, which for islands containing more than 15 atom rows along either [001] or $[1\bar{1}0]$ directions involves the formation of a thin, temporary domain wall. A noncollinear magnetic state is identified in a 7×7 atomic row Fe island where the magnetic moments are arranged in an antivortex configuration with the central ones pointing out of the (110) plane. This illustrates how the model can describe complicated exchange interactions even though it contains only a few parameters. The minimum energy path between this antivortex state and the collinear ground state is also calculated and the thermal stability of the antivortex state estimated.

PACS numbers: 05.20.Dd, 75.10.?b

I. INTRODUCTION

In theoretical studies of stable and metastable states of magnetic systems, the determination of magnetic forces is often required, i.e. the total energy gradient with respect to the orientation of the magnetic moments. Such forces are needed to calculate the dynamics of the system and to guide a minimization of the energy to identify stable or metastable magnetic states. Moreover, magnetic forces are particularly important for studying thermally activated magnetic transitions [1, 2], where a minimum energy path (MEP) connecting the initial and final states needs to be found. An MEP reveals the optimal mechanism of a transition, showing how each magnetic vector rotates so as to minimize the energy barrier to the transition. The highest energy point along the MEP represents a first order saddle point on the energy surface and can be used to estimate the activation energy for the transition. An efficient method for evaluating magnetic forces is essential for these kinds of calculations.

Density functional theory (DFT) can be used to study a wide range of magnetic systems. In the spin polarized extension using a 2×2 spin-density matrix, noncollinear states can be calculated and characterized [3]. Several studies of stationary magnetic states in various types of systems, including noncollinear systems, have been carried out using this approach [4]. Within an adiabatic approximation, the magnitude of the magnetic moments as well as the electronic charge in atomic volumes are assumed to be determined by the instantaneous orientation of the magnetic moments. The magnitude and electronic charge are determined using self-consistent, quantum mechanical calculations, while the orientation is treated classically [5]. The magnetic force giving the change in the energy with the direction of the magnetic moments can be calculated using a magnetic force theorem derived within the local spin density approximation (LSDA) to the exchange correlation functional [6–8]. This approach can, for example, be used to carry out simulations of spin dynamics using the Landau-Lifshitz equation of motion [5]. Such calculations are, however, quite involved and are computationally intensive. In order to describe nonstationary magnetic states, local constraints need to be introduced mimicking the effect of a local field acting on each magnetic moment so as to keep its orientation fixed in the predefined direction [9]. This local field needs to be determined self-consistently. An initial guess for the constraint is made, the system then relaxed subject to this constraint, the calculated orientation evaluated and compared with the predefined orientation, the constraint revised, etc. This adds

an inner self-consistency loop to the DFT calculations. As a result, the calculation of arbitrary nonstationary, noncollinear arrangements of the magnetic moments using DFT is challenging.

Most calculations of spin dynamics and magnetic transitions are presently carried out using simple, phenomenological models, in particular Heisenberg-type models, where the magnitude of the magnetic moments is assumed to be constant upon rotation. The determination of the total energy and its gradient with respect to orientation of the magnetic moments is then straightforward. However, in order to describe magnetic systems accurately enough, the model Hamiltonian may need to include several phenomenological terms. In addition to the usual magnetic exchange, anisotropy, dipole-dipole interaction, more elaborate interactions such as biquadratic exchange and Dzyaloshinsky-Moriya interaction have been invoked to better reproduce observed properties of magnetic systems [10]. The magnitude of the magnetic moments and interaction parameters in model Hamiltonians can, in principle, be calculated using DFT. Typically, this is done for collinear states [8, 11–13] and the parameters then kept the same for arbitrary noncollinear ordering of the magnetic moments. This approach can be accurate enough for small deviations from the collinear states, but is expected to fail for large rotation angles in itinerant electron systems [14] where the magnitude of magnetic moments and coupling parameters depend on the relative orientation of the moments. Sophisticated schemes have been proposed to make Heisenberg type models reproduce such behavior. Drautz and Fähnle [15] used a spin-cluster expansion to parametrize the total energy of a magnetic system as a function of orientation of the magnetic moments. Recently, Szilva *et al.* [16] derived an expression for the intersite exchange for an arbitrary alignment of spins making it easier to interpolate calculations for several points in configuration space. While additional parameters and elaborate expressions for the dependence of the parameters on the orientation of the magnetic moments can in principle be used to make a Heisenberg type model fit a given system, the transferability of the parameter values obtained in this way can be of concern and the question arises whether a different model that only requires a few, well defined parameters could be used instead.

The Alexander-Anderson (AA) model [17, 18] generalized to include multiple magnetic impurities describes magnetic systems containing itinerant electrons. It includes two electronic bands: a quasilocalized band of d-electrons and a band of itinerant $s(p)$ electrons. The model has been shown to give results that are consistent with DFT calculations but it

also provides a clear physical picture of the basic properties of the systems studied [19, 20]. A noncollinear extension of the AA model (NCAA) has been developed in mean-field approximation as well as an efficient implementation of the self-consistency calculations using the recursive Green function method [21, 22] and analytical transformations of the density of states [23, 24]. This makes it possible to apply the NCAA model to large and complex magnetic systems where a self-consistent calculation of the number of d electrons and magnitude of the magnetic moments is carried out for a fixed orientation of the magnetic moments. NCAA has, for example, been used successfully to describe magnetism of $3d$-metal surfaces and interfaces [23]. Moreover, a noncollinear ordering of magnetic moments in nanoclusters of $3d$-metal atoms was obtained in calculations using the NCAA model [25–27], and this prediction was later confirmed by DFT calculations [28, 29].

For an arbitrary, stationary or nonstationary orientation of the magnetic vectors, only the number of d electrons and the magnitude of magnetic moments are modified during the self-consistency calculations. The orientation of magnetic vectors remains unaffected, i.e. spin rotations are completely decoupled from the self-consistency procedure in the NCAA model. This is different from DFT calculations, where the orientation of magnetic moments at a nonstationary point is modified during a self-consistency calculation unless local constraining fields holding predefined magnetization direction are introduced [9].

The force acting on the orientation of the magnetic moments can be approximated using finite differences of the total energy evaluated for slightly different orientations. However, this is an inefficient approach as at least $2P + 1$ self-consistent calculations need to be carried out for each state of a system containing P magnetic moments. A more efficient, direct method for determining the force without additional self-consistency calculations is needed for large scale simulation of dynamics, optimization of transition paths, or, in general, navigation on the energy surface of a magnetic system. Analogous to the Hellmann-Feynman theorem [30] of quantum mechanics, force theorems have been derived within DFT formalism for the gradient with respect to the position of atomic nuclei [31] and, more importantly for the present case, orientation of magnetic moments [6–8]. We present here a magnetic force theorem for the NCAA model which not only makes it possible to calculate the energy gradient without repeated self-consistency calculations, but also provides a formula for the force acting on the orientation of the magnetic moments.

The article is organized as follows. In the following section, the NCAA model is briefly

described as well as the method used in the self-consistency calculations. In Sec. III, the magnetic force theorem is derived and the results used to obtain a formula for magnetic forces. In Sec. IV, the method is applied to a transition between parallel and antiparallel states in an Fe trimer and then to magnetization reversals in rectangular monolayer islands of Fe supported on W(110) surface. Finally, it is shown that a slightly different choice of the parameter values can lead to the appearance of a noncollinear metastable state with an antivortex structure [32] in a supported island. Section V gives a summary.

II. NONCOLLINEAR ALEXANDER-ANDERSON MODEL

The AA model [18] extended to multiple impurities and noncollinear ordering has been described elsewhere [24, 25], but for completeness and to define the notation needed for the following sections, a summary of the most important equations is given here. In the AA model, the electronic structure of a $3d$ transition metal is approximated by two bands: one representing quasilocalized d electrons and the other representing itinerant $s(p)$ electrons. The Hamiltonian for a system of P magnetic atoms is written as

$$\begin{aligned}\mathcal{H} = &\sum_{\mathbf{k},\alpha} \varepsilon_{\mathbf{k}} n_{\mathbf{k}\alpha} + \sum_{i,\alpha} \varepsilon_i^0 n_{i\alpha} + \sum_{\mathbf{k},i,\alpha} \left(v_{i\mathbf{k}} d_{i\alpha}^\dagger c_{\mathbf{k}\alpha} + v_{\mathbf{k}i} c_{\mathbf{k}\alpha}^\dagger d_{i\alpha} \right) \\ &+ \sum_{i \neq j,\alpha} v_{ij} d_{i\alpha}^\dagger d_{j\alpha} + \frac{1}{2} \sum_{i,\alpha} U_i n_{i\alpha} n_{i-\alpha}.\end{aligned} \tag{1}$$

Here $d_{i\alpha}^\dagger(d_{i\alpha})$ and $c_{\mathbf{k}\alpha}^\dagger(c_{\mathbf{k}\alpha})$ are creation (annihilation) operators for d electrons localized on atom i and itinerant $s(p)$-electrons with momentum $\mathbf{k}$, respectively; $n_{i\alpha} = d_{i\alpha}^\dagger d_{i\alpha}$, $n_{\mathbf{k}\alpha} = c_{\mathbf{k}\alpha}^\dagger c_{\mathbf{k}\alpha}$ are corresponding occupation number operators. Greek indices denote spin projection ($\alpha, \beta = \pm$). The energy of noninteracting $s(p)$ electrons, $\varepsilon_{\mathbf{k}}$, and d electrons, ε_i^0, hybridization parameters, $v_{i\mathbf{k}}$, hopping parameters, v_{ij}, and Coulomb repulsion between electrons with opposite spin projection, U_i, are spin independent. The last term in the Hamiltonian in Eq. (1), $U_i n_{i\alpha} n_{i-\alpha}$, describes interaction between d electrons at atom i, $i = 1, \ldots, P$.

The Hamiltonian in Eq. (1) is invariant with respect to the choice of quantization axis. In order to describe noncollinear magnetic states, we will use a mean-field approximation at each site i where a local quantization axis, z_i, is chosen to be along the local magnetic moment associated with atom i. The mean-field approximation for the last term in the

Hamiltonian is

$$n_{i\alpha}n_{i-\alpha} \approx n_{i\alpha}\langle n_{i-\alpha}\rangle + \langle n_{i\alpha}\rangle n_{i-\alpha} - \langle n_{i\alpha}\rangle\langle n_{i-\alpha}\rangle, \tag{2}$$

where $\langle n_{i\alpha}\rangle$ denotes the expectation value of an occupation number. The mean-field approximation is invoked at each site i for the electron operators $\tilde{d}^{\dagger}_{i\alpha}$ and $\tilde{d}_{i\alpha}$ whose quantization axis is z_i. In the end, the mean-field Hamiltonian can be rewritten in terms of $d^{\dagger}_{i\alpha}$ and $d_{i\alpha}$ where the quantization axis is taken to be the laboratory z-axis, the same for all sites i (this procedure is described in detail in [33], §2, for a similar Hamiltonian).

The d electrons are included explicitly here, while the influence of the itinerant $s(p)$-electrons is indirectly taken into account via the renormalization of model parameters. The mean-field Hamiltonian associated with the d electrons, $H \equiv \mathcal{H}^{(d)}_{MF}$, is given by

$$H = \sum_{i,\alpha} E^{\alpha}_i n_{i\alpha} + \sum_{i,j,\alpha,\beta} V^{\alpha\beta}_{ij} d^{\dagger}_{i\alpha} d_{j\beta} - \frac{1}{4}\sum_i U_i \left(N_i^2 - M_i^2\right), \tag{3}$$

where

$$E^{\alpha}_i = E^0_i + \frac{U_i}{2}\left(N_i - \alpha\cos\theta_i M_i\right), \tag{4}$$

$$V^{\alpha\beta}_{ij} = \frac{U_i}{2}\left(\delta^{\alpha\beta} - 1\right)\delta_{ij}\exp\left(-\alpha \mathrm{i}\phi_i\right)\sin\theta_i M_i + \left(1-\delta_{ij}\right)\delta^{\alpha\beta}V_{ij}. \tag{5}$$

Here, E^0_i is a renormalized energy of unperturbed d levels and V_{ij} are the hopping parameters that now contain both a contribution due to direct exchange between d states localized on sites i and j and a contribution from indirect d-d coupling through the conduction band. The choice of values for E^0_i and U_i depends mainly on the type of atom i, while the hopping parameters V_{ij} also depend on the geometry of the system, in particular the distance between atoms i and j. The hybridization of $s(p)$ and d bands leads to broadening of the d band and the width, Γ, is assumed to be a parameter in the model.

The polar angle θ_i and the azimuthal angle ϕ_i define the direction of the ith magnetic moment with respect to the laboratory quantization axis, z. In Eqs. (3)-(5), the number of d electrons, N_i, and the magnitude of magnetic moment, M_i, associated with one of the five degenerate d orbitals at atom i are

$$\begin{aligned} N_i &= \langle \tilde{d}^{\dagger}_{i+}\tilde{d}_{i+}\rangle + \langle \tilde{d}^{\dagger}_{i-}\tilde{d}_{i-}\rangle, \\ M_i &= \langle \tilde{d}^{\dagger}_{i+}\tilde{d}_{i+}\rangle - \langle \tilde{d}^{\dagger}_{i-}\tilde{d}_{i-}\rangle \end{aligned} \tag{6}$$

For a given orientation of the magnetic moments, specified by the angles θ_i and ϕ_i, the magnetic structure of a system of P metal atoms is described by a set of self-consistent values of N_i and M_i, where $i = 1, \ldots, P$.

The Green function $G(\omega)$, $G(\omega) = [\omega - H]^{-1}$, is used to obtain the self-consistency condition for N_i and M_i. According to Eqs. (6):

$$N_i = \frac{1}{\pi} \int_{-\infty}^{0} d\omega \, \mathrm{Im} \left[G_{ii}^{++}(\omega - i\Gamma) + G_{ii}^{--}(\omega - i\Gamma) \right], \tag{7}$$

$$\begin{aligned} M_i = & \frac{1}{\pi} \int_{-\infty}^{0} d\omega \, \mathrm{Im} \left[G_{ii}^{++}(\omega - i\Gamma) - G_{ii}^{--}(\omega - i\Gamma) \right] \cos\theta_i \\ & + \frac{1}{\pi} \int_{-\infty}^{0} d\omega \, \mathrm{Im} \left[G_{ii}^{+-}(\omega - i\Gamma) e^{i\phi_i} + G_{ii}^{-+}(\omega - i\Gamma) e^{-i\phi_i} \right] \sin\theta_i \end{aligned} \tag{8}$$

Here $G_{ii}^{\alpha\beta}(\omega)$ denotes a matrix element of the Green function. The magnetic system is assumed to be in contact with a large substrate which fixes the Fermi energy, for example a magnetic cluster or a thin film supported on a metal surface. The zero of energy is taken to be the Fermi energy ($\varepsilon_F = 0$).

When self-consistency is achieved, the total energy of d electrons can be found as

$$E = \frac{5}{\pi} \int_{-\infty}^{0} d\omega \omega \, \mathrm{Im} \, \mathrm{Tr} \, G^*(\omega - \mathrm{i}\Gamma) - 5 \sum_i \frac{U_i}{4} \left(N_i^{*2} - M_i^{*2} \right), \tag{9}$$

where the factor 5 is due to five-fold degeneracy of d orbitals. Quantities marked with an asterisk correspond to self-consistent values.

An integration over the density of d states needs to be carried out repeatedly in the self-consistency calculations (see Eqs. (7)-(8)). An efficient approach has been described in the literature [21, 22, 24]. First of all, the recursion method is applied in order to represent the Green function in terms of a continued fraction (see §3 in [21] and §2 in [22]). In Appendix A, we briefly describe how to obtain the continued fraction representation for the off-diagonal elements of the Green function. Then, the continued fraction is expanded in a series of partial fractions (see [24] and also Appendix B where the method is sketched), and a matrix element of the Green function then takes the form

$$G_{ij}^{\alpha\beta}(\omega) = \sum_k \frac{p_k}{\omega - q_k}, \tag{10}$$

where the numbers p_k, q_k depend on the orientation of the magnetic moments as well as on indices i, j and α, β. As a result, the density of states is expressed in terms of Lorentz profiles and can be integrated analytically.

The total energy of the system can be expressed analytically in terms of parameters of the self-consistent Hamiltonian as

$$\begin{aligned} E &= \frac{5}{\pi}\int\limits_{-\infty}^{0} d\omega\omega\Gamma\sum_{\mu=1}^{2P}\frac{1}{\left(\omega-\omega_\mu^*\right)^2+\Gamma^2} - 5\sum_{i=1}^{P}\frac{U_i}{4}\left(N_i^{*2}-M_i^{*2}\right) \\ &= \frac{5}{\pi}\sum_{\mu=1}^{2P}\left[\omega_\mu^*\,\mathrm{arcctg}\,\frac{\omega_\mu^*}{\Gamma}+\frac{\Gamma}{2}\ln\left(\frac{\omega_\mu^{*2}}{\Gamma^2}+1\right)\right] - 5\sum_{i=1}^{P}\frac{U_i}{4}\left(N_i^{*2}-M_i^{*2}\right), \end{aligned} \tag{11}$$

where ω_μ^* are the eigenvalues of H^*.

In self-consistency procedure, where the number of d electrons and magnitude of magnetic moments are found for an arbitrary orientation of magnetic vectors, we use a fundamental assumption about the hierarchy of relaxation time scales. Relaxation of the diagonal components of the spin density matrix, which in a local frame of reference give the number of d electrons and magnitude of magnetic moments, is much faster than the relaxation of the off-diagonal components which give the orientation of the magnetic moments [5]. Thus, N and M are treated as fast degrees of freedom which adjust instantaneously to the orientation of magnetic moments defined by polar and azimuthal angles $\boldsymbol{\theta}$ and $\boldsymbol{\phi}$, the slow degrees of freedom. This is analogous to the Born-Oppenheimer approximation in atomic systems where the electronic degrees of freedom are assumed to be fast as compared to slowly varying positions of nuclei, and the total energy of the system is expressed as a function of the slow degrees of freedom only.

III. MAGNETIC FORCE THEOREM

As discussed in the introduction, various calculation require the evaluation of the gradient of the total energy of the system which in the present case is the force acting on the orientation of the magnetic vectors. Below, we present a magnetic force theorem for the NCAA model which makes it possible to express the force in terms of self-consistent values of the number of d electrons,N^*, and modulus of the magnetic moment, M^*. The theorem is equivalent to a variational principle according to which self-consistency corresponds to a stationary point of the energy as a function of the fast degrees of freedom, N and M:

$$\forall i\colon \quad \left.\frac{\partial E}{\partial N_i}\right|_{\substack{N=N*\\M=M*}} = 0 \quad \text{and} \quad \left.\frac{\partial E}{\partial M_i}\right|_{\substack{N=N*\\M=M*}} = 0. \tag{12}$$

We will need two lemmas for the Green function that are proved in Appendix C:

$$\frac{\partial \operatorname{Tr} G(\omega)}{\partial N_i} = -\frac{U_i}{2}\frac{\partial}{\partial \omega}\left(G_{ii}^{++}(\omega) + G_{ii}^{--}(\omega)\right), \tag{13}$$

and

$$\begin{aligned}\frac{\partial \operatorname{Tr} G(\omega)}{\partial M_i} = \frac{U_i}{2}\frac{\partial}{\partial \omega}\big[&\left(G_{ii}^{++}(\omega) - G_{ii}^{--}(\omega)\right)\cos\theta_i \\ &+ \left(G_{ii}^{+-}(\omega)e^{i\phi_i} + G_{ii}^{-+}(\omega)e^{-i\phi_i}\right)\sin\theta_i\big].\end{aligned} \tag{14}$$

According to Eqs. (9) and (13)

$$\begin{aligned}\frac{\partial E}{\partial N_i} &= \frac{5}{\pi}\int\limits_{-\infty}^{0} d\omega\omega \operatorname{Im}\frac{\partial}{\partial N_i}\operatorname{Tr} G(\omega - \mathrm{i}\Gamma) - 5\frac{U_i}{2}N_i \\ &= 5\frac{U_i}{2}\left[\frac{1}{\pi}\int\limits_{-\infty}^{0} d\omega \operatorname{Im}\left(G_{ii}^{++}(\omega - \mathrm{i}\Gamma) + G_{ii}^{--}(\omega - \mathrm{i}\Gamma)\right) - N_i\right],\end{aligned}$$

where integration by parts is invoked. According to Eq. (7), the expression in the square brackets is equal to zero when self-consistency has been reached.

The equation for the derivative with respect to M_i in Eq. (12) is proved in the same way. Using (9) and (14), we obtain

$$\begin{aligned}\frac{\partial E}{\partial M_i} =& \frac{5}{\pi}\int\limits_{-\infty}^{0} d\omega\omega \operatorname{Im}\frac{\partial}{\partial M_i}\operatorname{Tr} G(\omega - \mathrm{i}\Gamma) + 5\frac{U_i}{2}M_i \\ =& 5\frac{U_i}{2}\Bigg\{-\frac{1}{\pi}\int\limits_{-\infty}^{0} d\omega \operatorname{Im}\big[\left(G_{ii}^{++}(\omega - \mathrm{i}\Gamma) - G_{ii}^{--}(\omega - \mathrm{i}\Gamma)\right)\cos\theta_i \\ &+ \left(G_{ii}^{+-}(\omega - \mathrm{i}\Gamma)e^{i\phi_i} + G_{ii}^{-+}(\omega - \mathrm{i}\Gamma)e^{-i\phi_i}\right)\sin\theta_i\big] + M_i\Bigg\}.\end{aligned}$$

Due to Eq. (8), the expression in the curly brackets is equal to zero when $M = M^*$.

The magnetic force theorem can be used to derive an expression for the force acting on the orientation of the magnetic moments within the NCAA model. According to the force theorem, a derivative of the energy, $E = E(\lambda)$, with respect to a parameter λ (a slow degree of freedom) can be computed from the explicit dependence only, without having to include implicit dependence

$$\frac{dE(\lambda)}{d\lambda} = \frac{\partial E(\lambda)}{\partial \lambda} = \frac{5}{\pi}\int\limits_{-\infty}^{0} d\omega\omega \operatorname{Im}\operatorname{Tr}\frac{\partial G^*(\omega - \mathrm{i}\Gamma;\lambda)}{\partial \lambda}. \tag{15}$$

Here, $\partial G^*(\omega - \mathrm{i}\Gamma;\lambda)/\partial\lambda$ can be found by using the resolvent identity

$$\frac{\partial G(\omega;\lambda)}{\partial\lambda} = G(\omega;\lambda)\frac{\partial H(\lambda)}{\partial\lambda}G(\omega;\lambda), \tag{16}$$

which, together with Eq. (15), gives

$$\begin{aligned}\frac{dE(\lambda)}{d\lambda} &= \frac{5}{\pi}\int_{-\infty}^{0} d\omega\omega\,\mathrm{Im}\,\mathrm{Tr}\left[G^*(\omega - \mathrm{i}\Gamma;\lambda)\frac{\partial H^*(\lambda)}{\partial\lambda}G^*(\omega - \mathrm{i}\Gamma;\lambda)\right] \\ &= \frac{5}{\pi}\int_{-\infty}^{0} d\omega\,\mathrm{Im}\,\mathrm{Tr}\left[G^*(\omega - \mathrm{i}\Gamma;\lambda)\frac{\partial H^*(\lambda)}{\partial\lambda}\right],\end{aligned} \tag{17}$$

that is, the derivative of the total energy with respect to a parameter coincides with the expectation value of the derivative of the Hamiltonian with respect to that parameter, analogous to the Hellmann-Feynman theorem [30].

In practice, it is convenient to calculate the trace in Eq. (17) using the basis in which $H^*(\lambda)$ and $G^*(\omega;\lambda)$ are diagonal

$$\mathrm{Tr}\left[G^*(\omega;\lambda)\frac{\partial H^*(\lambda)}{\partial\lambda}\right] = \sum_{\mu=1}^{2P}\frac{\xi_\mu^*}{(\omega - \omega_\mu^*)}, \tag{18}$$

where ξ_μ^* are the diagonal elements of $\partial H^*(\lambda)/\partial\lambda$ in the relevant basis. The integral in Eq. (17) can then be evaluated analytically leading to

$$\frac{dE(\lambda)}{d\lambda} = \frac{5}{\pi}\sum_{\mu=1}^{2P}\xi_\mu^*\,\mathrm{arcctg}\left(\frac{\omega_\mu^*}{\Gamma}\right). \tag{19}$$

With $\lambda = \theta_i$ or $\lambda = \phi_i$ and $i = 1,\ldots,P$, this gives the gradient of the energy with respect to the angles defining the orientation of the magnetic moments.

The procedure for evaluating the energy gradient is as follows: First, derivatives of the self-consistent Hamiltonian, $\partial H^*(\boldsymbol{\theta},\boldsymbol{\phi})/\partial\theta_i$ and $\partial H^*(\boldsymbol{\theta},\boldsymbol{\phi})/\partial\phi_i$, which are given explicitly by

$$\left(\frac{\partial H^*(\boldsymbol{\theta},\boldsymbol{\phi})}{\partial\theta_i}\right)_{kj}^{\alpha\beta} = \frac{1}{2}\delta_{ji}\delta_{ki}U_iM_i^*\left[\alpha\delta^{\alpha\beta}\sin\theta_i + \left(\delta^{\alpha\beta} - 1\right)\exp\left(-\alpha\mathrm{i}\phi_i\right)\cos\theta_i\right], \tag{20}$$

$$\left(\frac{\partial H^*(\boldsymbol{\theta},\boldsymbol{\phi})}{\partial\phi_i}\right)_{kj}^{\alpha\beta} = \frac{\mathrm{i}\alpha}{2}\left(1 - \delta^{\alpha\beta}\right)\delta_{ji}\delta_{ki}U_iM_i^*e^{-\alpha\mathrm{i}\phi_i}\sin\theta_i \tag{21}$$

are transformed to a basis where $H^*(\boldsymbol{\theta},\boldsymbol{\phi})$ is diagonal. Then, their diagonal matrix elements, $\xi_\mu^*(\theta_i)$, $\xi_\mu^*(\phi_i)$, are inserted into Eq. (19) and the derivatives with respect to θ and ϕ evaluated.

Thus, after self-consistency has been reached for an arbitrary, in general nonstationary, orientation of magnetic vectors, magnetic forces are readily available; no additional self-consistency calculations need to be performed. The forces can then be used to guide the orientation of magnetic vectors in spin dynamics simulations, minimization of the energy, or calculations of MEPs.

IV. APPLICATIONS

In what follows, we will demonstrate how the NCAA model and magnetic force theorem can be used to find (meta)stable magnetic states as well as MEPs for transitions between these states. Given some, possibly random initial values of the angles specifying the orientation of the magnetic moments, a steepest descent or, more efficiently, a conjugate gradient minimization of the energy can be used to find a configuration corresponding to a minimum on the energy surface, and thus a stable or metastable magnetic state. The ability to evaluate the gradient of the energy with respect to the angles specifying the orientation of the magnetic moments makes such calculations fast and reliable and improves the chances of finding novel and unexpected magnetic states. This is illustrated by an example below.

In order to assess the thermal stability of a magnetic state and to estimate the rate of transitions to other states, it is useful to find MEPs. An MEP shows how each magnetic moment rotates during the transition in an optimal way so as to make the energy barrier minimal. Thus, MEPs play a key role in the rate theory for magnetic transitions as they represent paths of highest statistical weight and reveal the transition mechanism and activation energy. The nudged elastic band (NEB) method can be used to find MEPs [34]. There, an initial path represented by a chain of intermediate states, or 'images', which give a discrete representation of the path, is created between a pair of stable states. An iterative algorithm involving force projections and a minimization algorithm is then used to bring the images to the nearest MEP. Each image is defined by a point in configuration space, i.e. by a set of angles $\boldsymbol{\theta}$ and $\boldsymbol{\phi}$ for each magnetic moment. In order to ensure continuity of the path and control the distribution of the images along the path, springs are introduced between adjacent images. At each step in the iteration, an estimate of the local tangent to the path at each image is made and the images moved only according to the perpendicular component of the force. In order to distribute the images in a predefined way along the path,

for example equally, a spring force is included between the images but only the component parallel to the path is included when the images are moved [34]. After convergence, when the projected forces are zero, the images give a discrete representation of the MEP. As the forces need to be evaluated repeatedly during this optimization procedure, the analytical expression based on the magnetic force theorem is of great importance.

A. Fe trimer on a metallic substrate

Previous studies have shown that ad-trimers of Fe, Cr and Mn can have several magnetic states that are close in energy [26]. We use a trimer to illustrate the methodology presented here because the energy surface with two magnetic states and the MEP connecting them can be visualized easily. The parameters in the NCAA model were chosen to be representative of an Fe trimer on a metal surface (see ref. [19] and references therein): $E^0/\Gamma = -12$ and $U/\Gamma = 13$. These values are only 5% different from values used to model bulk iron [19, 20, 23]. Here we have chosen unequal values for the three hopping parameters $V_{12}/\Gamma = 1.0$, $V_{13}/\Gamma = 1.19$ and $V_{23}/\Gamma = 1.22$ corresponding to an asymmetric geometry of the trimer.

Spin-orbit interaction is not taken into account in the NCAA model. The total energy of the system is, therefore, invariant under the uniform rotation of all the magnetic moments and only relative orientation of magnetic moments is relevant. Moreover, it is possible to show that the magnetic moments of all the atoms will tend to lie in a plane. The energy of the system increases significantly when one of the magnetic moments of an atom points out of a plane formed by the other two. Therefore, it is sufficient to set $\phi_i = 0$ for all three atoms to visualize the relevant part of the energy surface. It is convenient to choose the quantization axis for the system to be along the magnetic moment of one of the atoms, and a configuration of the system is then fully specified by only two angles, θ_2 and θ_3 between magnetic moments of the first and second atom and between first and third atom, respectively (see inset in Fig. 1(b)).

Fig. 1(a) shows a contour graph of the energy surface, $E(\theta_2, \theta_3)$. It has two minima, one at $\theta_2 = \theta_3 = 0$ and the other at $\theta_2 = \theta_3 = \pi$, and a maximum at $\theta_2 = 0$, $\theta_3 = \pi$. Both minima correspond to collinear spin states of the trimer. The lower energy state, P, has all magnetic moments pointing in the same direction, but the metastable state, AP, has the magnetic moment of the first atom pointing in the opposite direction to the other two. This

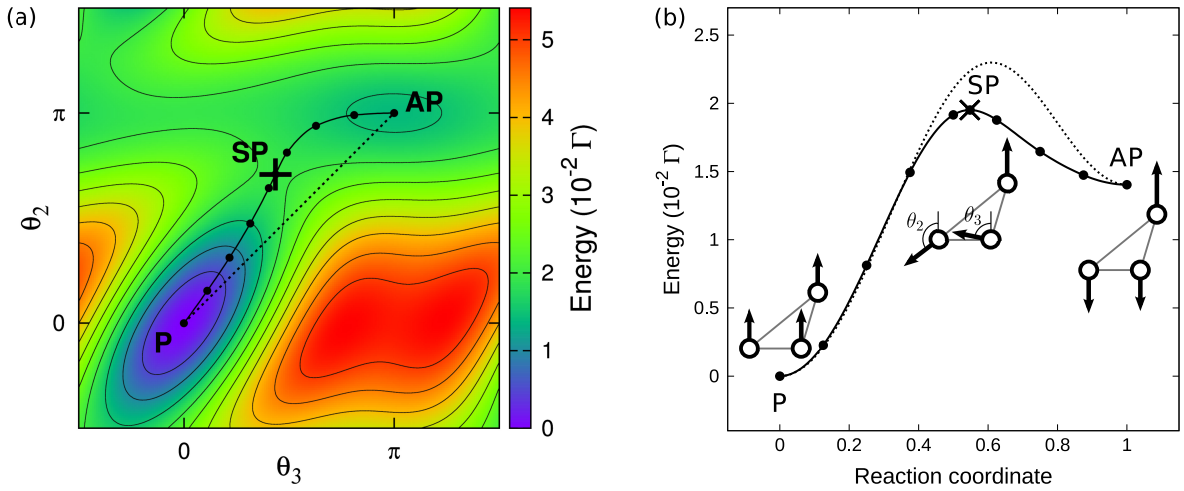

FIG. 1. The minimum energy path between two local minima on the energy surface corresponding to parallel (P) and antiparallel (AP) ordering of the spins is shown with a solid line. The filled circles show the location of images in a nudged elastic band calculation. × shows the location of the first order saddle point. The dotted line corresponds to the uniform rotation path. (a) Energy surface for an Fe trimer evaluated with the NCAA model. (b) Energy along the minimum energy and uniform paths. Insets show the direction and the magnitude of the magnetic moments at the minima and at the saddle point. The middle inset shows the definition of the angles θ_2 and θ_3. The reaction coordinate is defined as the sum of rotations of all magnetic moments along the path normalized by its total length.

is an example of a magnetic system with two possible states corresponding to two different arrangements of the magnetic vectors.

In the NEB calculations of the MEP, the initial path was chosen to correspond to uniform rotation. After convergence, the path lies through the first order saddle point on the energy surface and has a lower maximum than the uniform rotation path, see Fig. 1. Note that not only orientation of magnetic moments changes during the transition but also their magnitudes (see the insets in Fig. 1(b)).

Fig. 1(b) shows the variation in the total energy along the MEP. The energy maximum along the MEP corresponds to the first order saddle point on the energy surface. It gives an estimate of the activation energy barrier for magnetic transitions within harmonic transition state theory [2]. The barrier for the transition $P \rightarrow AP$ was found to be $E_{AP \leftarrow P} = E^S - E^P = 0.019\ \Gamma$, while for the reverse transition it is smaller, $E_{P \leftarrow AP} = E^S - E^{AP} = 0.005\ \Gamma$.

Energy variation for the uniform rotation of magnetic moments is also shown in Fig. 1(b) for comparison. This simple example illustrates the methodology which is applied to larger and more complex systems below.

B. Fe on W(110)

Recently, extensive experimental data on thermally induced magnetization reversals has been reported for monolayer Fe islands on W(110) surface [35]. We have, for comparison, used the methodology presented above to calculate the magnetism and rate of transitions in rectangular Fe islands of varying shape and size. Previously, a theoretical analysis using a Heisenberg-type Hamiltonian had been carried out [36], but here we present results using the NCAA model. A brief account of these calculations has been given elsewhere [37].

Since the NCAA model does not include spin-orbit coupling, it is necessary to supplement it with additional terms which introduce magnetic anisotropy. These terms describe the interaction of the magnetic system, here the Fe island, with the substrate and makes the magnetic vectors lie preferably along a particular direction within the surface plane. The total energy of the system is then

$$E = E^{NCAA} + \sum_n K_n \sum_i (\boldsymbol{M}_i \cdot \boldsymbol{e}_n)^2, \tag{22}$$

where E^{NCAA} is given by Eq. (11). The index n in the sum takes two values, $\parallel$ for easy-axis and $\perp$ for easy-plane anisotropy representing the interaction with the substrate. An easy-plane anisotropy $K_\perp$ is included to make it preferable for the magnetic moments to lie in the (110) plane. An easy-axis anisotropy $K_\parallel$ along the $[1\bar{1}0]$ direction is also included in order to give the system two degenerate magnetic states, with magnetic vectors aligned parallel or antiparallel to this axis. The parameter values were chosen to be $K_\perp \mu_B^2 = 0.7\ meV$ and $K_\parallel \mu_B^2 = -0.3$ meV. A wide range of values for $K_\perp$ suffices to keep the magnetic moments within the surface plane, but the value of $K_\parallel$ was chosen to get roughly the experimentally determined magnitude for the activation energy of magnetization reversals in Fe islands on W(110).

Although magnetostatic dipole-dipole interaction was included in our previous study using a Heisenberg-type model [36], its contribution to the activation energy of the magnetization reversal was less than 0.5%. The size of the Fe islands studied here is less than 6

nanometers. At this length scale, dipole-dipole interaction is irrelevant and, therefore, not included here.

The parameters E^0/Γ and U/Γ in the NCAA model were chosen to have the same values as for the trimer, but the V/Γ and Γ parameters were chosen to reproduce results of DFT calculations of an Fe monolayer on W(110), as described below.

1. Fe monolayer on W(110)

An Fe monolayer on the W(110) surface is commensurate with the substrate. Each Fe atom in the layer has four nearest neighbors at a distance of $0.87a$, where a is the lattice constant of the W crystal and two second nearest neighbors at a slightly larger distance, a (see the inset in Fig. 2). The hopping parameter corresponding to the first nearest neighbors was chosen to have the value $V^{(1)}/\Gamma = 0.9$ where $\Gamma = 0.2$ eV. For simplicity, the hopping parameters for further neighbors were set to zero. This value of Γ agrees well with the width of the *d*-band subpeaks in the density of states calculated with DFT, and with this value of $V^{(1)}/\Gamma$, the calculated magnetic moment is $2.4\mu_B$ reproducing the results of DFT calculations [38]. Even though only nearest neighbor hopping parameters are non-zero, there is still exchange coupling between second and farther neighbors in the NCAA model because each pair of moments interacts due to indirect coupling through intermediate atoms. In order to demonstrate this, we calculated the exchange parameters, J_{0j}, for a collinear ground state, where indices 0 and j label atoms as illustrated in the inset in Fig. 2. If the polar axis is chosen to be perpendicular to the (110) surface, then the exchange parameters are defined as

$$J_{0j} = -\frac{\partial^2 E}{\partial\phi_0 \partial\phi_j}$$

and were evaluated by finite differences of the calculated gradients after small rotations.

The exchange coupling calculated for a monolayer of Fe on a W(110) surface using the NCAA model is in good agreement with results of DFT calculations [39]. In both cases, ferromagnetic exchange coupling is obtained between first nearest neighbors, while antiferromagnetic exchange coupling is obtained between the second nearest neighbors (see Fig. 2 and Fig. 1 in ref. [39]). For more distant neighbors, this parametrization of the NCAA model, however, gives $J_{03} = J_{02}$, while the DFT results show a significant difference between the two. If additional parameters are included in the NCAA model, for example $V^{(2)}/\Gamma = 0.3$

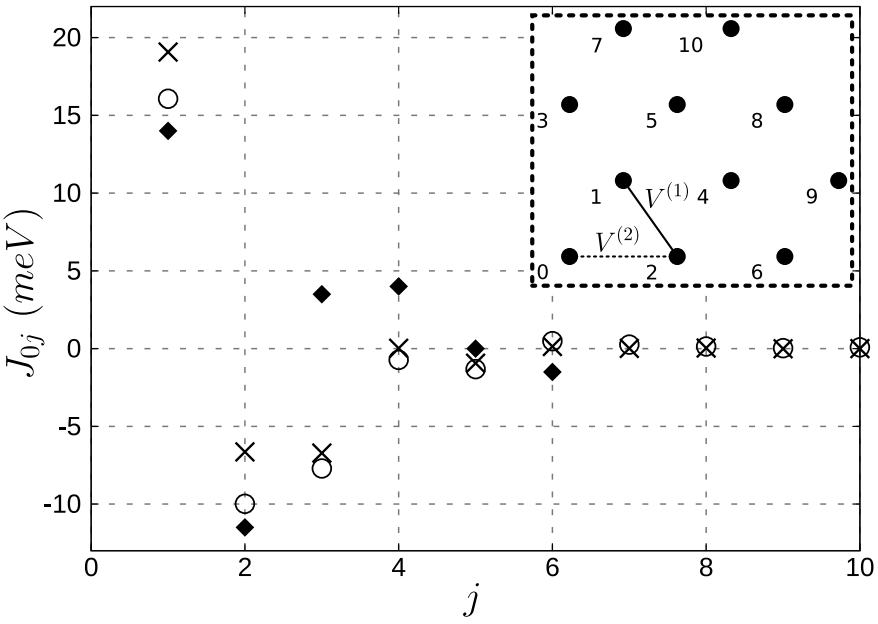

FIG. 2. Exchange interaction parameters for a monolayer of Fe-atoms on W(110) in the collinear ground state. (Crosses) show results obtained when only nearest-neighbor hopping parameter is nonzero, $V^{(1)}/\Gamma = 0.9$ (circles) show results obtained when also second nearest-neighbor hopping is included, $V^{(2)}/\Gamma = 0.3$. (Diamonds) show results of density functional theory calculations presented in ref. [39]. The ferromagnetic coupling between nearest neighbors and antiferromagnetic coupling between second-nearest neighbors is nicely reproduced in the NCAA model, even when only nearest-neighbor hopping parameters are included. The inset shows the position of neighbors j relative to atom 0 and illustrates the definition of the hopping parameters.

for direct hopping between second nearest neighbors, then the values of J_{02} and J_{03} become different as shown in Fig. 2 and agreement with DFT results for J_{01} and J_{02} is improved. In what follows, we will, however, use the simplest possible parametrization of the NCAA and include only the hopping parameter between nearest neighbors, $V^{(1)}/\Gamma = 0.9$. This gives good agreement with the DFT results for the magnitude of the magnetic moment as well as the most important exchange coupling, between nearest neighbors and between second nearest neighbors. More elaborate parametrization of the NCAA model could be undertaken but will not be pursued here.

2. Fe islands on W(110)

Calculations using the NCAA model with the parameters described above were carried out for monolayer, rectangular islands of Fe-atoms of varying shape and size. As an example, the magnetic moments obtained from the self-consistent calculations of a 29×5 atomic row island are shown in Fig. 3. The value obtained for the innermost atoms is nearly the same as for the full monolayer, but the atoms at the rim of the island have about 10% larger magnetic moment. In between, the atoms have a slightly smaller value than atoms in a full monolayer. The increased magnetic moment at the rim atoms can explain in part island size dependence of the activation energy for magnetization reversals, as discussed below.

3. Magnetization reversal

There are two degenerate magnetic states of the islands, where all the magnetic vectors point in one of the two directions along the anisotropy axis. Thermally induced magnetization reversal transitions between these two states were studied by calculating MEPs, as described for the trimer above. The orientation of the magnetic moment of each atom was included explicitly. Two mechanisms for magnetization reversal were found. Small islands, with fewer than 15 atomic rows, reverse their magnetization by coherent rotation of all the magnetic moments. However, transitions in islands with more than 15 atomic rows along either side follow a more complicated path involving nucleation and propagation of an excitation that can be described as a thin, temporary domain wall. This is similar to what we previously found in calculations using a Heisenberg-type Hamiltonian [36] and what has been seen in atomistic spin dynamics simulations of similar systems [40, 41]. Fig. 3 shows results for a 29×5 atomic-row island which contains 72 Fe-atoms. It turns out that the variation in the magnitude of the magnetic moments along the MEP calculated self-consistently with the NCAA model is small, lending support for the application of a Heisenberg-type Hamiltonian to study such transitions. The magnetization reversal starts at one of the narrower ends of the island and a domain wall forms parallel to the short axis of the island. The domain wall then moves along the [001] direction eventually leading to reversal of the magnetization of the whole island. Fig. 3 shows the energy along the MEP. The height of the energy barrier is determined by the domain wall length which in this case scales with the size of the island

along the [1$\bar{1}$0] direction. The energy change for a uniform rotation of magnetic moments is also shown in Fig. 3 for comparison. This shows how much the formation of the transient domain wall lowers the activation energy of the transition.

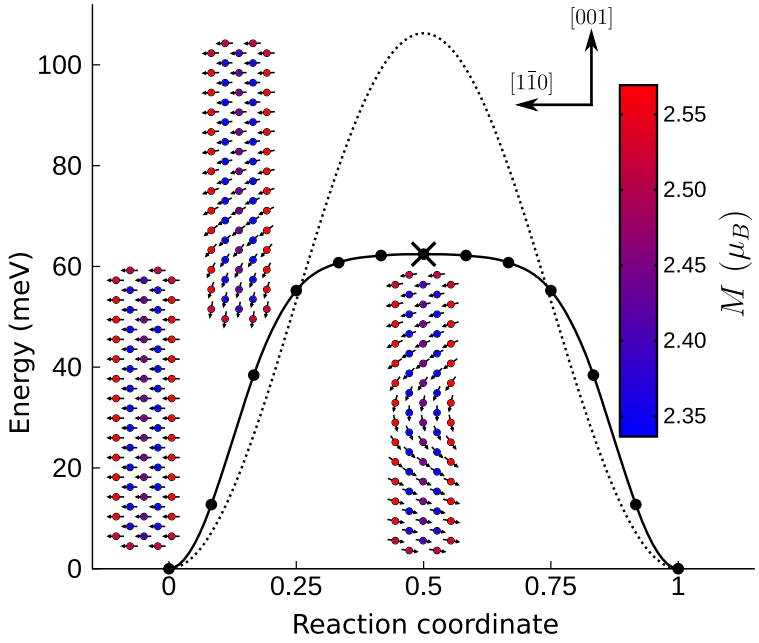

FIG. 3. Magnitude of the magnetic moment of Fe-atoms in a 29 × 5 atomic row island on W(110) surface, calculated using the NCAA model, and energy change along the MEP (solid line) for a magnetization reversal. The energy maximum along the MEP, which corresponds to a saddle point on the energy surface, is marked with a ×. The energy change for a uniform rotation of magnetic moments is also shown (dotted line). The reaction coordinate is defined as the normalized displacement along the path. The orientation of crystallographic axes, [1$\bar{1}$0] and [001], are indicated with arrows. The anisotropy axis, $K_{\|}$, is oriented along the [1$\bar{1}$0] direction. Insets show the direction and magnitude of the magnetic moments at the energy minimum, at the saddle point and at another intermediate configuration.

The ca. 10% larger magnetic moment of the rim atoms as compared with the innermost atoms does, however, lead to some difference from the results obtained using a Heisenberg-type Hamiltonian [36], where the magnitude of the magnetic moments is taken to be the same for all atoms. Fig. 4 compares the calculated energy barrier as a function of the size of the islands, L, along the [1$\bar{1}$0] direction obtained using the Heisenberg-type Hamiltonian (results are taken from Ref. [36]) and the NCAA model. The number of atomic rows along the [001]

direction equals 27 and is kept constant. For a vanishing domain wall length (the intercept with the y-axis), the Heisenberg-type model predicts zero activation energy barrier, but the NCAA model gives an offset of about 18 meV. This offset appears because the rim atoms have larger anisotropy energy due to the larger magnetic moment. As the islands become smaller, the relative number of rim atoms increases. This leads to a larger activation energy for the small islands as compared to what the Heisenberg-type model predicts, where the anisotropy is the same for all atoms in the island.

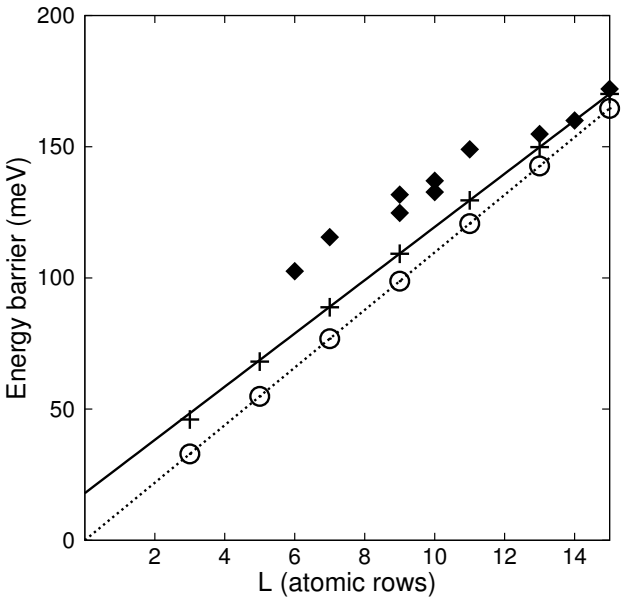

FIG. 4. Energy barrier to magnetization reversal in rectangular islands of Fe-atoms on W(110) surface as a function of the island size, L, along the $[1\bar{1}0]$ direction calculated using the NCAA model (crosses) and Heisenberg-type Hamiltonian (circles; data taken from Ref. [36]). The length of the islands along the [001] direction is 27 atom-rows in all cases. Solid and dotted lines represent linear fits, giving an extrapolation to islands with zero width, i.e. the intercept. Diamonds show experimentally measured energy barriers for islands which have a more irregular shape, see ref. [35].

Such an offset has, in fact, been observed experimentally [35], see Fig. 4, lending support for the NCAA model results. The offset obtained from the measurements is, however, about three times larger than the one obtained from our simple model. Several effects not included in the calculations could contribute to this difference, such as (1) irregular shape of the islands measured experimentally where larger number of atoms are at the rim than in the rectangular islands of the calculation, (2) broken symmetry in the spin-orbit interaction at

the edges of islands leading to larger anisotropy, or (3) impurity adatoms sitting preferably either on rim atoms or on interior atoms (but not both) [42].

4. An antivortex metastable state

The analytical forces provided by the force theorem make it easier to navigate on the energy surface to find local minima, corresponding to (meta)stable magnetic states with possibly complex, non-collinear ordering of magnetic moments. Starting from a random initial orientation of the magnetic moments, a steepest descent or conjugate gradient minimization of the energy will bring the system to a (meta)stable state. This procedure reveals metastable states which could be hard to find otherwise. We demonstrate this with a small island having 7x7 atomic rows. Two of the parameters in the NCAA model have here been changed slightly: The energy of the d level with respect to the Fermi energy was changed from $E^0/\Gamma = -12$ to -11.9, and the hopping parameter between nearest neighbors was changed from $V^{(1)}/\Gamma = 0.9$ to 1.025. Such a slight change in the model parameters could be the result of an external perturbation such as an external electrical field or the presence of impurities or defects [42]. It does not lead to significant changes in the magnetic moments and exchange coupling. For the Fe monolayer on W(110) in the collinear ferromagnetic state, the magnetic moment increases by only $0.01\mu_B$. Also, the exchange interaction parameters J_{0j} do not change much, except for J_{02} and J_{03}, which change from $-6.7\ meV$ to $-10\ meV$. However, this slight change in E^0/Γ and $V^{(1)}/\Gamma$ is large enough to have a significant effect on the magnetic structure of Fe nanoislands on W(110).

Ten minimization calculations were carried out starting from different, random orientations of the 24 magnetic moments. In three of these calculations, a noncollinear state with an antivortex spin structure was found (see Fig. 5). The collinear ground state was found in the other seven calculations. The metastable antivortex state can be described as a symmetrical, saddlelike arrangement of the magnetic moments in the center of the island. The total in-plane magnetization is zero, while the out-of-plane magnetization is nonzero mainly due to four magnetic moments near the center of the island which point out of the (110) plane. The identification of this magnetic state illustrates the power of the methodology described above, which is efficient because of the magnetic force theorem.

Magnetic antivortices have been identified before (see, for example, [32]), but those are

much larger than the one we found here. Typically, the formation of an antivortex state is closely related to the magnetostatic interaction, which is usually negligible on the nanoscale. Here, the antivortex state demonstrates the complex exchange interaction which is included in the NCAA model even though it contains only a few parameters. The trimer example discussed above, see Fig. 1, shows that both parallel and antiparallel alignment of magnetic moments is possible in a system without anisotropy. Such a behavior cannot be obtained within a Heisenberg-type model unless additional phenomenological terms and additional parameters are introduced in the Hamiltonian. In the NCAA model, complex noncollinear states appear quite naturally.

An NEB calculation was carried out to estimate the thermal stability of the antivortex state. The MEP for the transition from this state to the collinear ground state is shown in Fig. 5. The saddle-like excitation moves along the diagonal of the island towards one of the corners (the upper right corner in the insets of Fig. 5) where it leaves the island. The activation energy for the transition from the metastable state to the ground state was calculated to be 10 meV, while for the reverse transition it is 55 meV.

V. SUMMARY

We have derived in this paper a magnetic force theorem for the NCAA model. According to this theorem, derivatives of the total energy with respect to the number of d electrons and magnitude of magnetic moments vanish when self-consistency has been reached. As a result, the energy gradient with respect to the orientation of magnetic moments or, more generally, any adiabatic parameter, can be computed without having to repeat the self-consistency calculations. This theorem is of great practical importance as it significantly reduces the computational effort involved in finding magnetic states, calculating MEPs between the states, simulating spin dynamics and, more generally, navigating on the energy surface.

The theorem can also be used to calculate magnetic exchange parameters, J_{ij}, for an arbitrary, noncollinear ordering of magnetic moments, by using finite differences of the forces. In general, the exchange coupling depends on orientation of magnetic moments and cannot be reduced to a bilinear term only [43, 44]. Thus the NCAA model can account for a complex, non-Heisenberg magnetic exchange coupling, which could play an important role in the formation of exotic, noncollinear states, such as the antivortex state found here. It

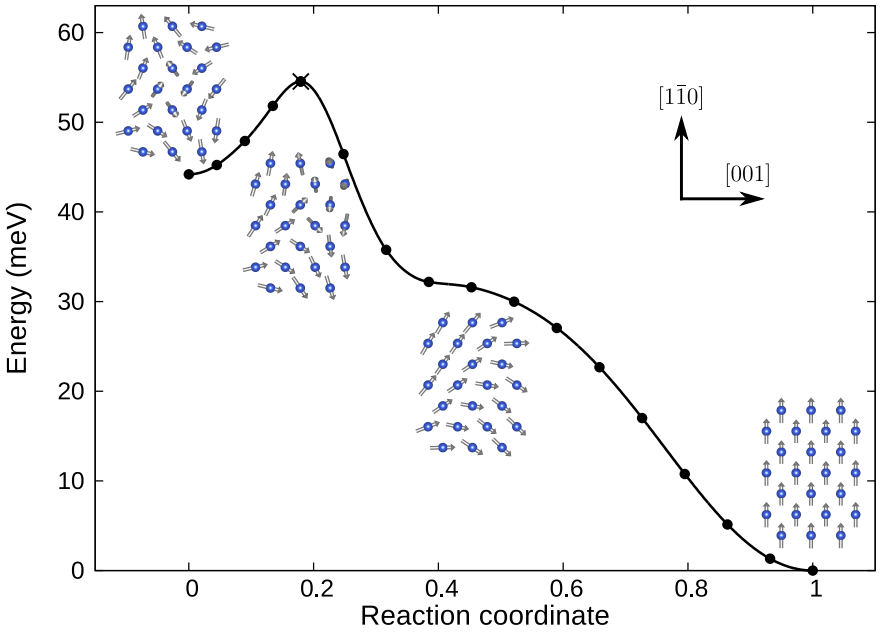

FIG. 5. Energy along the minimum energy path between an antivortex metastable state and the collinear ground state of an Fe-island with 7×7 atomic rows. The energy maximum along the path, which corresponds to a first order saddle point on the energy surface, is marked with a $\times$. The reaction coordinate is defined as the normalized displacement along the path. The orientation of crystallographic axes, $[1\bar{1}0]$ and [001], are indicated with arrows. The anisotropy axis, $K_{\|}$, is oriented along the $[1\bar{1}0]$ direction. Insets show the direction and magnitude of the magnetic moments at the minimum energy configurations, at the saddle point and at another intermediate configuration.

may even be possible to form magnetic skyrmions [10] within the NCAA model.

ACKNOWLEDGMENTS

This work was supported by the Government of Russian Federation (Grant No. 074-U01), RFBR Grant No. 14-02-00102, the Icelandic Research Fund, and the Nordic-Russian Training Network for Magnetic Nanotechnology (NCM-RU10121).

Appendix A: Continued-fraction expansion for the off-diagonal elements of the Green function

In the original method due to Haydock [21, 22], the continued-fraction representation is obtained for the diagonal elements of the Green function. The recursion method, however, can also be applied to the off-diagonal elements, $G_{\mu\nu}(\omega) = \langle x_\mu | \, G(\omega) \, | x_\nu \rangle$, $\mu \neq \nu$, where $|x_\mu\rangle$ and $|x_\nu\rangle$ are the members of an initial basis set, and indices μ, ν enumerate both atomic site and spin projection.

In Haydock's method, a basis set is found that tridiagonalizes the Hamiltonian. All members of that basis set as well as matrix elements of the tridiagonal Hamiltonian are found systematically after specifying the first vector, $|y_1\rangle$. The matrix element $\langle y_1 | \, G(\omega) \, | y_1 \rangle$ is then expressed in terms of a continued fraction. The choice of $|y_1\rangle$ in this procedure is arbitrary.

In order to find $G_{\mu\nu}(\omega)$, a tridiagonalization is performed four times, where the starting vectors are:

$$
\begin{aligned}
|y_1^a\rangle &= \frac{1}{\sqrt{2}} \left(|x_\mu\rangle + |x_\nu\rangle \right), \\
\left|y_1^b\right\rangle &= \frac{1}{\sqrt{2}} \left(|x_\mu\rangle - |x_\nu\rangle \right), \\
|y_1^c\rangle &= \frac{1}{\sqrt{2}} \left(|x_\mu\rangle + \mathrm{i} \, |x_\nu\rangle \right), \\
\left|y_1^d\right\rangle &= \frac{1}{\sqrt{2}} \left(|x_\mu\rangle - \mathrm{i} \, |x_\nu\rangle \right).
\end{aligned}
$$

In each basis, matrix element $\tilde{G}_{11}^{\zeta}(\omega) = \left\langle y_1^{\zeta} \right| G(\omega) \left| y_1^{\zeta} \right\rangle$, $\zeta = a, b, c, d$, is expanded in terms of continued fraction as described in Refs. [21, 22]. Continued-fraction representation for the real and imaginary part of the nondiagonal element, $G_{\mu\nu}(\omega)$, is thus given by:

$$
\operatorname{Re} G_{\mu\nu}(\omega) = \frac{1}{2} \left(\tilde{G}_{11}^{a}(\omega) - \tilde{G}_{11}^{b}(\omega) \right), \tag{A1}
$$

$$
\operatorname{Im} G_{\mu\nu}(\omega) = \frac{1}{2} \left(\tilde{G}_{11}^{d}(\omega) - \tilde{G}_{11}^{c}(\omega) \right). \tag{A2}
$$

Appendix B: Partial-fraction expansion of the Green function

In the recursion method, matrix elements of the Green function are expressed in terms of continued fractions of the following kind:

$$C(\omega) = \cfrac{1}{\omega - a_1 - \cfrac{|b_1|^2}{\omega - a_2 - \cfrac{\cdots}{\cdots - \cfrac{|b_{2P-1}|^2}{\omega - a_{2P}}}}} \tag{B1}$$

The method developed in Ref. [24] involves systematically reducing the number of levels in the continued fraction, starting from the last level. Here, we briefly describe the idea of this method. Let us consider the last level of the continued fraction, Eq. (B1):

$$f^{(1)}(\omega) = \omega - a_{2P-1} - \frac{|b_{2P-1}|^2}{\omega - a_{2P}}. \tag{B2}$$

If $b_{2P-1} \neq 0$, then the equation $f^{(1)}(\omega) = 0$ has two real roots, $q_1^{(2)}$ and $q_2^{(2)}$, $q_1^{(2)} < q_2^{(2)}$, which can be found either analytically or numerically. Then

$$f^{(1)}(\omega) = \frac{\left(\omega - q_1^{(2)}\right)\left(\omega - q_2^{(2)}\right)}{\omega - q_1^{(1)}},$$

where $q_1^{(1)} \equiv a_{2P}$. As a result, the next level of the continued fraction acquires the form:

$$f^{(2)}(\omega) = \omega - a_{2P-2} - \frac{|b_{2P-2}|^2 \left(\omega - q_1^{(1)}\right)}{\left(\omega - q_1^{(2)}\right)\left(\omega - q_2^{(2)}\right)} = \omega - a_{2P-2} - \frac{p_1^{(2)}}{\omega - q_1^{(2)}} - \frac{p_2^{(2)}}{\omega - q_2^{(2)}}, \tag{B3}$$

where $p_1^{(2)}$ and $p_2^{(2)}$ are defined as

$$p_1^{(2)} = |b_{2P-2}|^2 \frac{q_1^{(2)} - q_1^{(1)}}{q_1^{(2)} - q_2^{(2)}}, \qquad p_2^{(2)} = |b_{2P-2}|^2 \frac{q_2^{(2)} - q_1^{(1)}}{q_2^{(2)} - q_1^{(2)}},$$

Thus function $f^{(2)}(\omega)$ is represented in a form which is analogous to Eq. (B2), and the number of levels in the continued fraction is reduced by one. The same technique is used in order to successively eliminate all levels of $C(\omega)$. At each step k, finding zeros of $f^{(k)}(\omega)$ does not cause problems, because they are well separated.

Appendix C: Proof of lemmas (13) and (14)

In this appendix, we sketch the proof of the lemmas (13) and (14), which can be written as

$$\frac{\partial \operatorname{Tr} G(\omega)}{\partial N_i} = -\frac{U_i}{2} \frac{\partial}{\partial \omega} \left(G_{ii}^{++}(\omega) + G_{ii}^{--}(\omega) \right), \tag{C1}$$

$$\frac{\partial \operatorname{Tr} G(\omega)}{\partial M_i} = \frac{U_i}{2}\frac{\partial}{\partial \omega}\left[\left(G_{ii}^{++}(\omega) - G_{ii}^{--}(\omega)\right)\cos\theta_i + \left(G_{ii}^{+-}(\omega)e^{i\phi_i} + G_{ii}^{-+}(\omega)e^{-i\phi_i}\right)\sin\theta_i\right]. \tag{C2}$$

Due to the resolvent identity, we have:

$$\frac{\partial G(\omega)}{\partial N_i} = G(\omega)\frac{\partial H}{\partial N_i}G(\omega), \tag{C3}$$

$$\frac{\partial G(\omega)}{\partial M_i} = G(\omega)\frac{\partial H}{\partial M_i}G(\omega). \tag{C4}$$

It follows directly from Eq. (3) that

$$\left(\frac{\partial H}{\partial N_i}\right)_{kj}^{\alpha\beta} = \frac{U_i}{2}\delta^{\alpha\beta}\delta_{ki}\delta_{ji}, \tag{C5}$$

$$\left(\frac{\partial H}{\partial M_i}\right)_{kj}^{\alpha\beta} = \frac{U_i}{2}\delta_{ki}\delta_{ji}\left[-\alpha\delta^{\alpha\beta}\cos\theta_i + \left(\delta^{\alpha\beta}-1\right)\sin\theta_i e^{-\alpha \mathrm{i}\phi_i}\right]. \tag{C6}$$

Using Eqs. (C3), (C5) and invariance of a trace under cyclic permutations we get:

$$\frac{\partial \operatorname{Tr} G(\omega)}{\partial N_i} = \operatorname{Tr} G^2(\omega)\frac{\partial H}{\partial N_i} = -\operatorname{Tr}\frac{\partial G(\omega)}{\partial \omega}\frac{\partial H}{\partial N_i} = -\frac{U_i}{2}\left(\frac{\partial G_{ii}^{++}(\omega)}{\partial \omega} + \frac{\partial G_{ii}^{--}(\omega)}{\partial \omega}\right), \tag{C7}$$

where use was made of the following identity:

$$\frac{\partial G(\omega)}{\partial \omega} = -G^2(\omega).$$

Eq. (C7) proves lemma (C1). Lemma (C2) is proven in the same way. We have:

$$\frac{\partial \operatorname{Tr} G(\omega)}{\partial M_i} = \operatorname{Tr} G^2(\omega)\frac{\partial H}{\partial M_i} = -\operatorname{Tr}\frac{\partial G(\omega)}{\partial \omega}\frac{\partial H}{\partial M_i} = \frac{U_i}{2}\left[\left(\frac{\partial G_{ii}^{++}(\omega)}{\partial \omega} - \frac{\partial G_{ii}^{--}(\omega)}{\partial \omega}\right)\cos\theta_i + \left(\frac{\partial G_{ii}^{+-}(\omega)}{\partial \omega}e^{i\phi_i} + \frac{\partial G_{ii}^{-+}(\omega)}{\partial \omega}e^{-i\phi_i}\right)\sin\theta_i\right], \tag{C8}$$

which proves lemma (C2).

---

[1] G. Fiedler, J. Fidler, J. Lee, T. Schrefl, R. L. Stamps, H. B. Braun and D. Suess, *J. Appl. Phys.* **111**, 093917 (2012).

[2] P.F. Bessarab, V.M. Uzdin, H. Jónsson, Phys. Rev. B **85**, 184409 (2012).

[3] U. von Barth and L. Hedin, Journal of Physics C: Solid State Physics **5**, 1629 (1972).

[4] G. Bihlmayer, 'Density-functional theory of magnetism', in *'Handbook of magnetism and advanced magnetic materials'*, ed. H. Kronmüller and S. Parkin. Vol. 1, page 3.

[5] V.P. Antropov, M.I. Katsnelson, B.N. Harmon, M. van Schilfgaarde, D. Kusnezov, Physical Review B **54**, 1019-1035 (1996).

[6] A.I Liechtenstein, M.I. Katsnelson, V.A. Gubanov, Journal of Physics F: Metal Physics **14**, L125-L128 (1984).

[7] A. Oswald, R. Zeller, P.J. Braspenning, P.H. Dederichs, Journal of Physics F: Metal Physics **15**, 193-212 (1985).

[8] A.I Liechtenstein, M.I. Katsnelson, V.P. Antropov, V.A. Gubanov, Journal of Magnetism and Magnetic Materials **67**, 65-74 (1987).

[9] G. M. Stocks , B. Ujfalussy , Xindong Wang , D. M. C. Nicholson , W. A. Shelton , Yang Wang , A. Canning and B. L. Györffy, Philosophical Magazine Part B **78**, 665 (1998).

[10] S. Heinze, K. von Bergmann, M. Menzel, J. Brede, A. Kubetzka, R. Wiesendanger, G. Bihlmayer, S. Blügel, Nature Physics **7** 713 (2011).

[11] L. Udvardi, L. Szunyogh, K. Palotás, and P. Weinberger, Physical Review B **68**, 104436 (2003).

[12] G.H.O. Daalderop, P.J. Kelly, M.F.H. Schuurmans, Physical Review B **41**, 11919-11937 (1990).

[13] G. Wu, K.H. Khoo, M.H. Jhon, H. Meng, S.Y.H. Lua, R. Sbiaa, C.K. Gan, Europhysics Letters **99**, 17001 (2012).

[14] S. Lounis, P.H. Dederichs, Physical Review B **82**, 180404(R) (2010).

[15] R. Drautz and M. Fähnle, Physical Review B **69**, 104404 (2004).

[16] A. Szilva, M. Costa, A. Bergman, L. Szunyogh, L. Nordström, O. Eriksson, Physical Review Letters **111**, 127204 (2013).

[17] P.W. Anderson, Physical Review **124**, 41-53 (1961).

[18] S. Alexander, P.W. Anderson, Physical Review **133**, A1594-A1603 (1964).

[19] V.M. Uzdin, A. Vega, A. Khrenov, W. Keune, V.E. Kuncser, J.S. Jiang,and S.D. Bader, Phys. Rev. B **85**, 024409 (2012).

[20] V.M. Uzdin, H. Zabel, A. Remhof, B. Hjörvarsson, Phys. Rev. B **80**, 174418 (2009).

[21] R. Haydock, V. Heine, M.J. Kelly, Journal of Physics C: Solid State Physics **5**, 2845-2858 (1972).

[22] R. Haydock, V. Heine, M.J. Kelly, Journal of Physics C: Solid State Physics **8**, 2591-2605 (1975).

[23] S.V. Uzdin, Physics of the Solid State **51**, 1260-1270 (2009).

[24] V.M. Uzdin, N.S. Yartseva, Computational Materials Science **10**, 211-216 (1998).

[25] S. Uzdin, V. Uzdin, C. Demangeat, Europhysics Letters **47**, 556-561 (1999).

[26] S. Uzdin, V. Uzdin, C. Demangeat, Surface Science **482**, 965-969 (2001).

[27] S. Uzdin, V. Uzdin, C. Demangeat, Computational Materials Science **17**, 441-444 (2000).

[28] H.J. Gotsis, N. Kioussis, D. A. Papaconstantopoulos, Physical Review B **73**, 014436 (2006).

[29] A. Bergman, L. Nordström, A.B. Klautau, S. Frota-Pessôa, O. Eriksson, Physical Review B **73**, 174434 (2006).

[30] P. Güttinger, Z. Phys. **73**, 169 (1932); H. Hellmann, *Einführung in die Quantenchemie* (Deuticke, Leipzig, 1937), pp. 61 and 285; R.P. Feynman, Ph.D. thesis, Massachusetts Institute of Technology, 1939; Phys. Rev. **56**, 340 (1939).

[31] A.R. Mackintosh and O.K. Andersen, in *Electrons at the Fermi Surface*, edited by M. Springford (Cambridge University Press, Cambridge, England, 1980), p. 149; V. Heine, Solid State Phys. **35**, 1 (1980); M. Methfessel and J. Kubler, J. Phys. F **12**, 141 (1982); M. Weinert, R.E. Watson, and J.W. Davenport, Phys. Rev. B **32**, 2115 (1985).

[32] B. Van Waeyenberge, A. Puzic, H. Stoll, K.W. Chou, T. Tyliszczak, R. Hertel, M. Fähnle, H. Brückl, K. Rott, G. Reiss, I. Neudecker, D. Weiss, C.H. Back, G. Schütz, Nature **444**, 461 (2006).

[33] K. Hirai, Journal of The Physical Society of Japan **61**, 2491-2502 (1992).

[34] H. Jónsson, G. Mills, K. W. Jacobsen, 'Nudged Elastic Band Method for Finding Minimum Energy Paths of Transitions', in *'Classical and Quantum Dynamics in Condensed Phase Simulations'*, ed. B. J. Berne, G. Ciccotti and D. F. Coker (World Scientific, 1998), page 385; G. Henkelman and H. Jónsson, *J. Chem. Phys.* **113**, 9978 (2000).

[35] S. Krause, G. Herzog, T. Stapelfeldt, L. Berbil-Bautista, M. Bode, E. Y. Vedmedenko, and R. Wiesendanger, Phys. Rev. Lett. **103**, 127202 (2009).

[36] P.F. Bessarab, V.M. Uzdin and H. Jónsson, Phys. Rev. Letters **110**, 020604 (2013).

[37] P.F. Bessarab, V.M. Uzdin and H. Jónsson, Zeitschrift für Physikalische Chemie **227**, 1543

(2013).

[38] A.T. Costa, R.B. Muniz, J.X. Cao, R.Q. Wu and D.L. Mills, Phys. Rev. B **78** 054439 (2008).

[39] A. Bergman, A. Taroni, L. Bergqvist, J. Hellsvik,B. Hjörvarsson, O. Eriksson, Physical Review B **81**, 144416 (2010).

[40] D. Böttcher, A. Ernst, J. Henk, J. Phys.: Condens. Matter **23**, 296003 (2011).

[41] D.S.G. Bauer, P. Mavropoulos, S. Lounis, S. Blügel, J. Phys.: Condens. Matter **23**, 394204 (2011).

[42] P.F. Bessarab, V.M. Uzdin and H. Jónsson, Phys. Rev. B **88**, 214407 (2013).

[43] P.F. Bessarab, M.G. Dudnik, V.M. Uzdin, Bulletin of the Russian Academy of Sciences: Physics **77**, 56 (2013).

[44] A.T. Costa, Jr., R.B. Muniz, D.L. Mills, Phys. Rev. Lett. **94** 137203 (2005).